

# Angular-spectral antenna effects in ultra wideband communications links

W.Q. Malik, D.J. Edwards and C.J. Stevens

**Abstract:** In traditional approaches to antenna characterisation, spectral and angular dispersion are modelled separately. In the paper, the dependence of the power radiated from ultra wideband (UWB) antennas jointly on frequency and direction is established experimentally. It is demonstrated that both omni-directional and directional antennas typically exhibit higher directivity with frequency, with the former experiencing a seven-fold increase with respect to the lowest frequency in the FCC UWB frequency range (3.1–10.6 GHz). The consequences of this behaviour are highlighted and the effect on the communications link is quantified. The effective available bandwidth of a system is found to be highly sensitive to the angular disposition of the antenna at each end of the link. It is shown that the bandwidth is severely limited in some directions, and careful orientation of the antennas is required to achieve full UWB operation for a range of antenna designs. The 10 dB bandwidth of a vertically polarised UWB antenna can be as little as 2 GHz in the equatorial plane when the joint dispersion is considered. The distortion caused to a UWB signal is investigated and significant variation in the radiated signal waveform with angle is demonstrated.

## 1 Introduction

Ultra wideband (UWB) communications technology provides unprecedented data rates over a short distance supporting high capacity links and large user densities [1]. With other favourable characteristics such as unlicensed spectrum usage, low power consumption, and little multi-user interference, it holds great promise for some next generation communications applications. UWB systems are characterised by their large fractional or absolute bandwidths [2]. The current Federal Communications Commission (FCC) regulations in the US provide for a 7.5 GHz band for unlicensed indoor wireless communications [3]. This bandwidth far exceeds the coherence bandwidth of the indoor radio channel, resulting in frequency-selective behaviour [4, 5]. The antenna is an integral part of a wireless system and a well-designed antenna is critical for system performance. UWB antenna design requires careful modelling of its performance as part of the communications link. Many types of UWB antennas have been proposed in literature, and designs such as the biconical, bowtie, d-dot, log-spiral, Vivaldi, TEM horn and ridged circular horn are among the most popular [6–11].

Traditional antenna characterisation is centred around fundamental antenna parameters related to the input characteristics and radiation patterns [12]. While this is usually sufficient for narrowband antennas, several issues arise in the case of UWB antennas that merit deeper analysis. The end-to-end signal distortion introduced by the

transmitter and receiver UWB antennas is effectively a filtering operation such that the antenna response is convolved with the signal waveform. The physical size and shape of the antenna also affects its time-frequency response. For example, a log-periodic antenna disperses a UWB signal as the low frequency signal components are launched earlier than the high frequency components, where the connection to the transmission line is at the broad end [13]. In such case, the phase centre of the antenna translates with frequency resulting in temporal distortion [14]. This form of distortion can be described in terms of the group delay through time-domain transient response analysis [15, 16].

Apart from these, the frequency dependence of the radiated power as defined by the Friis transmission equation [17] for freespace propagation also causes waveform distortion owing to non-uniform power flux density across the UWB band. After transmission and reception through the antennas, the UWB signal power spectrum slope is determined by the antenna combination [18, 19]. This can be interpreted as a differentiation or integration operation in the time domain [20], introducing phase shifts and waveform distortion in the signal [21], and is thus highly detrimental to the performance of both single-band and multi-band UWB communications links [22]. The characterisation of frequency dependence of various antenna parameters is thus of paramount importance for UWB system design.

Besides spectral and temporal dispersion, angle is another domain where the behaviour of an antenna can have a significant impact. This is particularly important for indoor communications systems such as wireless personal area networks, where dense multipath propagation gives rise to a wide range of angles of arrival [23–25]. In the absence of the theoretical isotropic radiator, a broadcast transmitter using an omni-directional antenna is expected to radiate the signal in all directions within the azimuthal plane with symmetric

© IEE, 2006

IEE Proceedings online no. 20050048

doi:10.1049/ip-com:20050048

Paper first received 31st January and in final revised form 29th August 2005

The authors are with Department of Engineering Science, University of Oxford, Parks Road, Oxford OX1 3PJ, UK

E-mail: wasim.malik@eng.ox.ac.uk

gain and group delay such that the wavefronts have near-uniform intensity and planar shapes. In practice, however, this condition is sometimes violated by UWB antennas, causing look-angle dispersion [14].

Instead of analysing the frequency and look-angle distortion separately, this paper jointly investigates the angular and spectral dispersive effects of UWB antennas. The variation of antenna radiation patterns with frequency is first established with the simple example of a dipole antenna, and is then evaluated experimentally using discone [26, 27] and Vivaldi [28–31] antennas that represent the general cases of omni-directional and directional UWB antennas respectively. To quantify the radiation pattern variation with frequency, the antenna beam area and directivity are calculated as functions of frequency. The effect of this behaviour on the available system bandwidth is quantified in terms of the effective angular bandwidth, and the distortion caused to a generic UWB waveform is evaluated. While the details of the dispersive behaviour will vary from antenna to antenna, the results of this paper illustrate the phenomenon and highlight its consequences without loss of generality.

## 2 Dipole radiation patterns

The dipole is inherently a narrowband antenna but is representative of many other, more complex antenna shapes [12]. Also, its field equations are analytically tractable and well understood. On the basis of its compact, simple and economical design, the dipole has been suggested for use in short-range UWB transmission [32]. For a vertically oriented dipole, the elevation plane far-field radiation pattern can be expressed in terms of the angle of elevation  $\theta$  and frequency  $f$  as

$$F(\theta, f) = \frac{\cos\left(\frac{kl}{2}\right) - \cos\left(\frac{kl \sin \theta}{2}\right)}{\cos \theta} \quad (1)$$

where  $l$  is its length,  $k = 2\pi/\lambda$  is the wavenumber and  $\lambda$  is the wavelength. For a 0.1 m long dipole, the power radiation pattern varies significantly within the FCC-allocated UWB band (3.1–10.6 GHz). This is shown in Fig. 1, where the normalised elevation plane radiation patterns at four equidistant frequencies within that band are plotted. An increase in operating frequency leads to higher directivity and an increase in the number of lobes. The directions of the lobes also change with frequency, increasing in elevation.

This observation points to the important problem of frequency-dependent antenna radiation in UWB communications. The following Sections probe the existence of similar phenomena in some specialised UWB antennas and evaluate their performance for the transmission and reception of a signal comprising a large frequency content.

## 3 Antenna measurements

The discone is a popular choice of antenna for omni-directional, linearly polarised systems. With a conveniently manufactured design and bandwidth exceeding a decade [27, 33], it is popular for conducting UWB channel measurements in the laboratory [34, 35]. The radiation pattern of the discone is similar to electrically small dipole, biconical, and bowtie antennas [36]. For directional propagation, aperture antennas such as the Vivaldi and various horn designs can be used. The Vivaldi antenna,

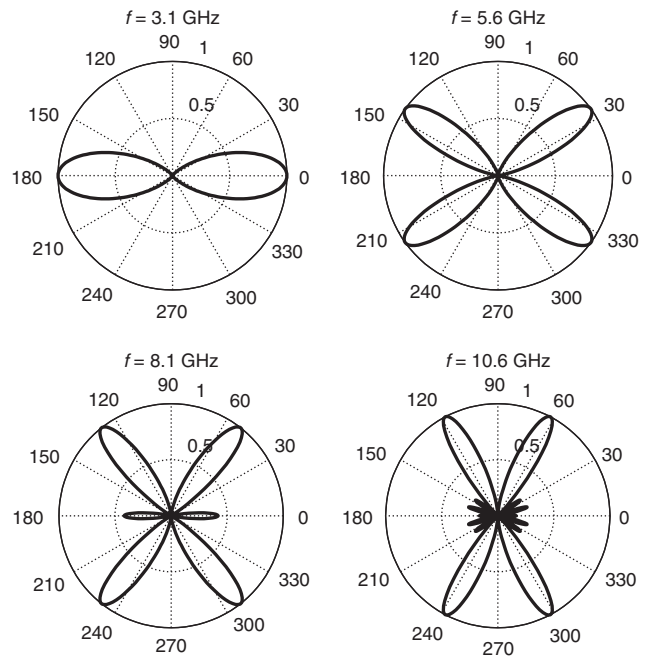


**Fig. 1** Normalised elevation plane field radiation patterns of a vertically polarised dipole antenna at various frequencies, with the circular axis signifying the variation along the elevation

an elliptically tapered slotline structure, has been shown to yield good broadband performance [31].

A pair of identical Vivaldi antennas was manufactured using a photolithographic process, while the discones were made by machining. Each discone antenna, made from aluminium, consisted of a hollow cone and a large circular ground plane, with its geometry described by the cone length  $l = 0.065$  m, cone half-angle  $\psi = 45^\circ$ , and ground plane diameter  $d = 0.2$  m, as shown in Fig. 2a. The balanced antipodal Vivaldi antenna, shown in Fig. 2b, had dimensions of  $d = 0.04$  m and  $l = 0.1$  m. An elliptically tapered slotline structure, it had a triplanar form with two layers of dielectric sandwiched between three layers of duroid substrate.

Both pairs of antennas were extensively characterised in an anechoic chamber. A vector network analyser (VNA) was used to measure the  $S_{11}(f)$  parameter of the scattering matrix  $S$ . The VNA was calibrated prior to the measurement to remove the attenuation, delay and phase distortion of the cables and connectors. The  $S_{11}(f)$  is used to derive the reflection coefficient  $\Gamma(f)$ , which yields the antenna return loss in logarithmic scale often used to characterise the radiation performance of an antenna over a given frequency band. Figure 3 shows the reflection loss of the four antennas. For the discone antennas, the reflection loss lies well below  $-10$  dB for the entire UWB band, i.e.  $f_l = 3.1$  to  $f_h = 10.6$  GHz. This is also true for the Vivaldi except for a small range of frequencies near 9 GHz, owing to which the radiation efficiency of these Vivaldi antennas is higher in the lower portion of the UWB band. Furthermore, the corresponding antennas have similar  $\Gamma(f)$ , which confirms that the antennas of each type are identical.

The power radiation patterns were measured in the anechoic chamber using the setup shown in the plan view in Fig. 4. A set of  $n_f = 16$  discrete equidistant frequencies within the UWB band were measured with a continuous-wave signal generator and power metre, providing a frequency resolution of  $\Delta_f = 500$  MHz. Both antennas were placed on electromagnetic absorbent blocks to prevent any

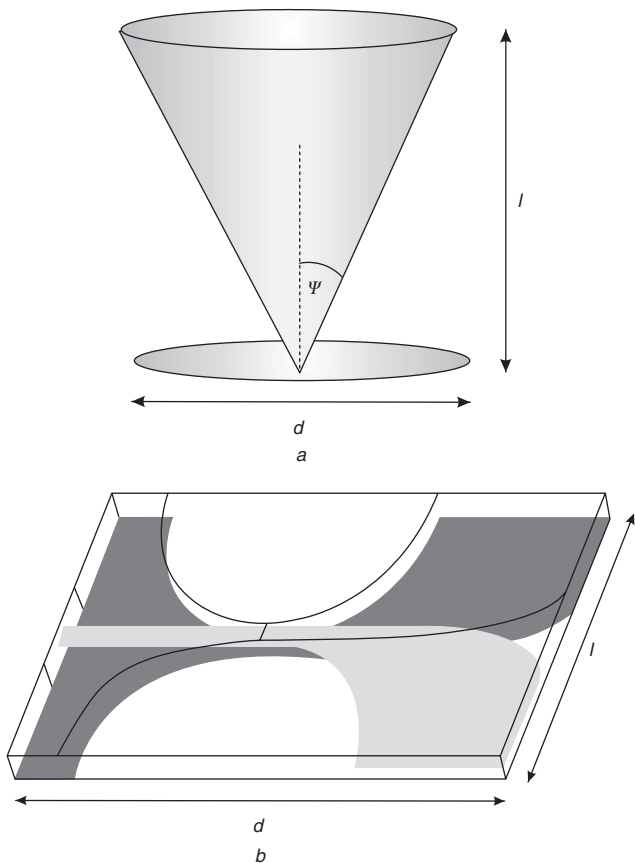


**Fig. 2** Construction of UWB antennas  
*a* Discone antenna with a large circular ground plane  
*b* Balanced antipodal Vivaldi antenna

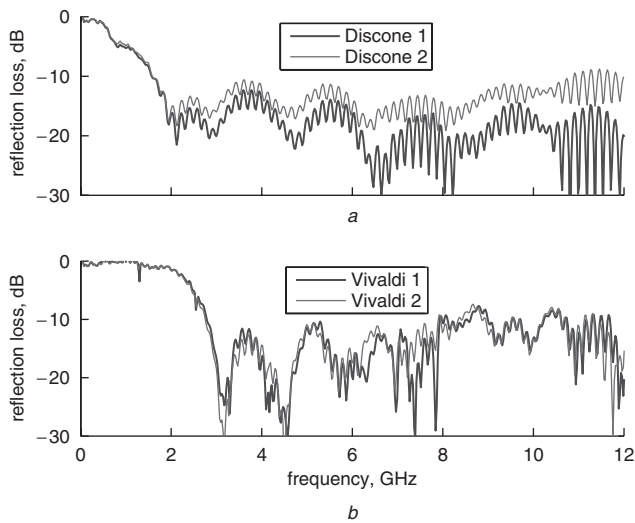


**Fig. 3** Measured reflection loss  
*a* Discone  
*b* Vivaldi antennas

ground reflections, and were separated by a distance of  $r = 2.85$  m. The transmitted power was  $P_t = 15$  dBm, and a low-noise amplifier with 30 dB gain was connected to the receiving antenna. The transmitting antenna was fixed at one position while the receiving antenna was placed on a computer-controlled turntable and rotated in the elevation,  $\theta$ , and azimuth,  $\phi$ , planes from  $0^\circ$  to  $360^\circ$  with angular resolution  $\Delta\theta = \Delta\phi = 1^\circ$ .

Consider the rotation of the receiving antenna by an angle  $\alpha_r$  while the transmitter is stationary at  $\alpha_t = 0^\circ$ , with

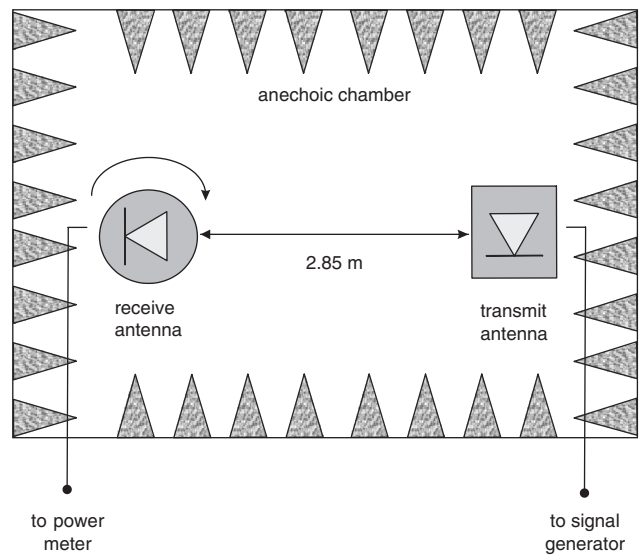


**Fig. 4** Antenna radiation pattern measurement in an anechoic chamber

the antenna separation  $r$  kept constant. According to the Friis equation [17], the received power is a function of the product of the antenna gains

$$P_r(\alpha, f) = G_t(\alpha_t, f)G_r(\alpha_r, f) \quad (2)$$

where  $G_t(\alpha_t, f)$  and  $G_r(\alpha_r, f)$  are the gains of the transmitting and receiving antennas respectively,  $\lambda$  is the wavelength corresponding to  $f$ , and the transmitted power and free-space loss terms have been neglected. With one stationary antenna, the received power can be represented by

$$P_r(\alpha, f) = G(\alpha, f)G(0, f) \quad (3)$$

where  $G_t(\alpha, f) = G_r(\alpha, f) = G(\alpha, f)$  for the identical antennas. It is straightforward to see that

$$G(0, f) = \sqrt{P_r(0, f)} \quad (4)$$

so that the gain of a single antenna-under-test can be derived from the received power as

$$G(\alpha, f) = \frac{P_r(\alpha, f)}{\sqrt{P_r(0, f)}} \quad (5)$$

This procedure is used to obtain the multi-frequency radiation patterns,  $P(\theta, \phi, f)$ , of the antenna in the elevation and azimuth planes. Normalisation with the highest received signal intensity removes the effect of the radiator-sensor separation and provides the radiation patterns used subsequently, i.e.

$$P_n(\theta, \phi, f) = \frac{P(\theta, \phi, f)}{\sup_{\theta, \phi} \{P(\theta, \phi, f)\}} \quad (6)$$

#### 4 UWB antenna radiation patterns

To develop an insight into the radiation characteristics of these UWB antennas, the power radiation patterns of the discone and Vivaldi antennas are studied in this Section. The discone is linearly polarised, circularly symmetric and omni-directional in the azimuthal plane. The far-field elevation pattern of a thin discone resembles that of a monopole, but for large values of the cone half-angle  $\psi$ , the presence and number of any sidelobes depends on  $\psi$ . The electrical length of the cone  $k_l = 2\pi/l$  determines the cutoff frequency and the elevation plane beam pattern. The ground plane introduces a slant to the

elevation pattern depending on the electrical diameter  $k_d = 2\pi/d$  and frequency  $f$ .

The Vivaldi antenna is a stripline-to-freespace transformer with a very broadband input match. Its radiation pattern, however, is expected to vary considerably with frequency as the phase centre shifts within the structure. The advantage of the design is that maximum gain is maintained in the boresight direction. The lower cutoff frequency of the Vivaldi is determined by the flare angle, such that the aperture is half a wavelength wide at that frequency.

Figure 5 shows the normalised, co-polar power radiation patterns of the discone and Vivaldi antennas in the elevation and azimuth planes across the UWB band. According to the definition of the angles in the Figure, the discone elevation boresight is nominally at  $\pm 90^\circ$ , and for the Vivaldi it is at  $0^\circ$ . Keeping in view the range of the radiated power, the images are thresholded to a lower level of  $-15$  dB.

From Figure 5a, the discone antenna has an elevation-plane radiation pattern that evolves with frequency. There is very low power when the two discone antennas are perpendicular to each other, as expected. Towards the lower end of the band, a large, well-defined mainlobe is

observed close to the equatorial direction. Considerable radiation is also present at a wide range of angles owing to the flow of current to the edges of the ground plane, since  $d \approx 2\lambda$  at low  $f$ . With increasing frequency, the boresight pattern contracts and translates, while the backplane propagation vanishes. The most noticeable changes close to the 6 GHz, beyond which the beam diverges, and the mainlobe continues to narrow. For  $\lambda < l$ , the antenna starts behaving like a multiple-wavelength monopole instead of a quarter-wave monopole, resulting in narrower beams and an increase in the number of sidelobes and nulls [12]. The sidelobes are produced by the reflection of the wave from the discontinuity at the far end of the finite cone as explained in [37], where the relationship of antenna dimensions with beamwidth, beam tilt and sidelobe level is discussed for a finite, large-angle conical antenna without a ground plane.

The discone's azimuth radiation pattern in Fig. 5b is uniform with the elevation angle as expected for an omni-directional antenna, but there is considerable variation with  $f$  owing to the non-uniform return loss and antenna efficiency.

The Vivaldi antenna's elevation pattern in Fig. 5c and azimuth pattern in Fig. 5d both show strong boresight gain.

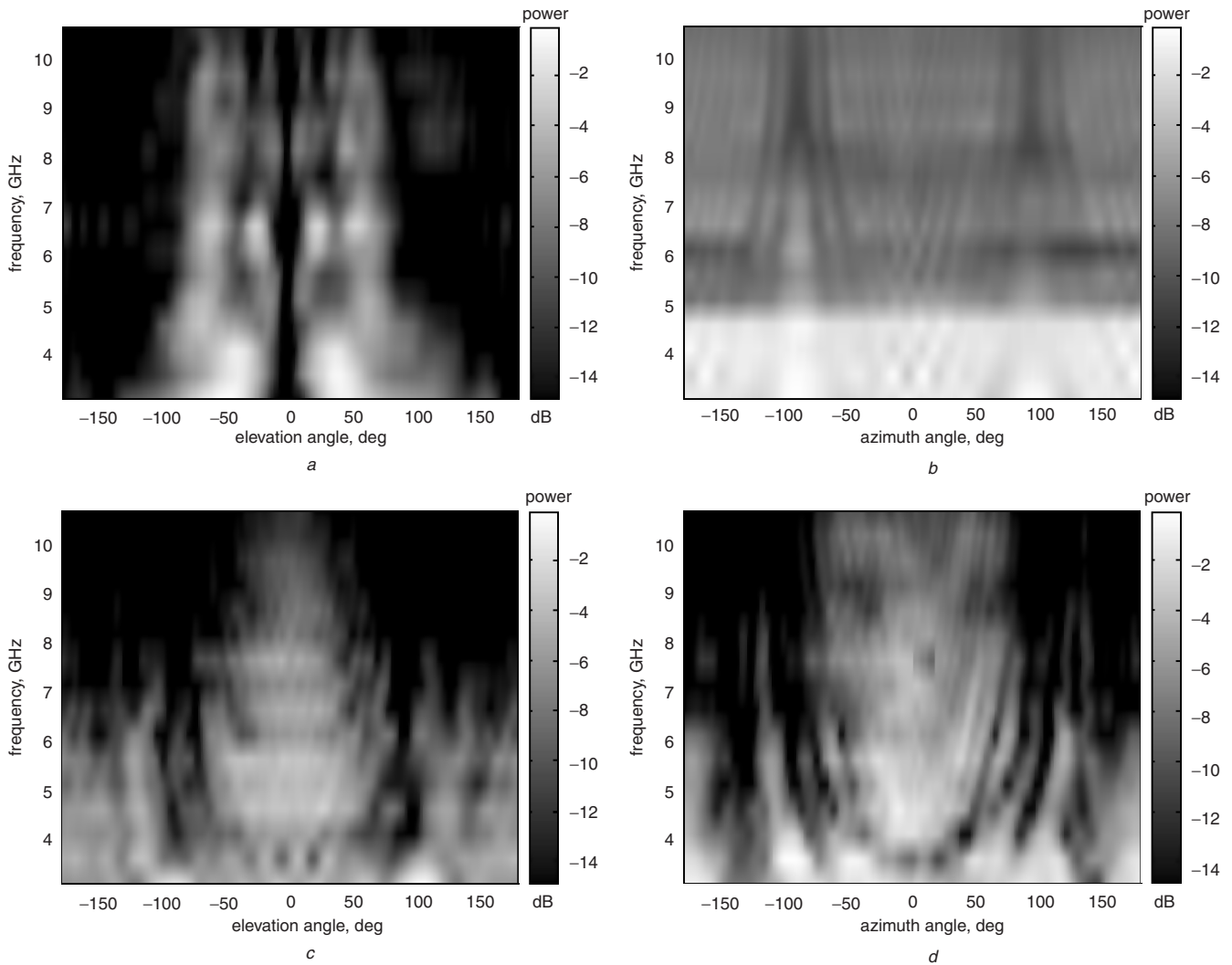


**Fig. 5** Evolution of UWB antenna radiation patterns with frequency  
*a* Discone, elevation plane  
*b* Discone, azimuth plane  
*c* Vivaldi, elevation plane  
*d* Vivaldi, azimuth plane

At the lower end of the spectrum there is appreciable backplane propagation, especially in the case of the elevation pattern which is nearly omni-directional up to the centre frequency. The desired angular discrimination is achieved only at high frequencies. The elevation mainlobe narrows with increasing  $f$  and the sidelobes vanish. The azimuth pattern has more ripples than the elevation pattern, indicating greater leakage through sidelobes, which decay at lower frequencies for most angles.

Thus the elevation radiation pattern of the discone antenna is strongly dependent on frequency. The antenna's frequency properties at one look-angle are starkly different from those at another. Alternatively, the frequency components are radiated non-uniformly in different directions. In a typical indoor wireless application, a terminal using the discone antenna in a vertically polarised configuration held by a user sitting down would experience a different frequency response, and thus performance, than while standing. Also, it is common to place the transmitting and receiving antennas in the horizontal plane. In such a situation, a signal with only a subset of the frequencies will be launched in the antenna plane, while a wider range of frequencies might be available at a steeper angle. All of these effects will cause waveform distortion and power loss in single-band UWB systems, while in multi-band systems, the antenna efficiency in a given sub-band will vary substantially with the look-angle.

## 5 Radiation properties

The antenna beamwidth and directivity can be used to quantify the angular-spectral variation of UWB antennas as observed in the previous Section. The mainlobe beamwidth can be evaluated in terms of the beam solid angle

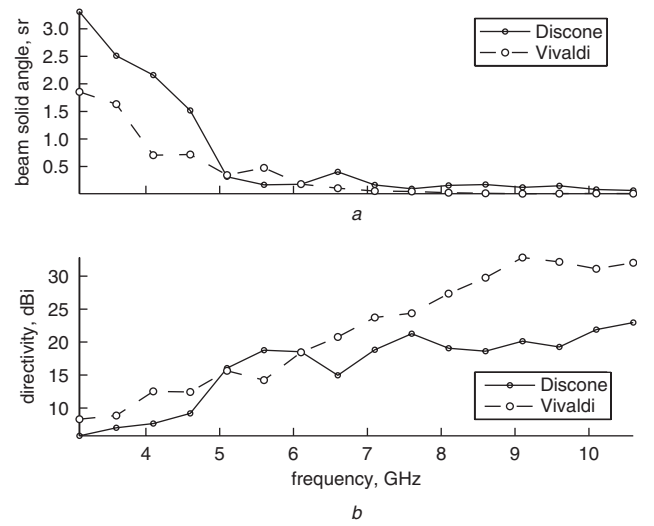
$$\begin{aligned}\Omega_A(f) &= \int_0^{2\pi} \int_0^\pi P_n(\theta, \varphi, f) d\Omega \\ &= \int_0^{2\pi} \int_0^\pi P_n(\theta, \varphi, f) \sin \theta d\theta d\varphi\end{aligned}\quad (7)$$

Figure 6a shows the beam solid angle of the discone and Vivaldi antennas. Both have a large beam solid angle at low frequencies, lying in the region of 2–3 sr, which falls exponentially with frequency in a nearly identical fashion for the two antennas reaching 0.1 sr at  $f_h$ . Even though the beam solid angle of the Vivaldi remains smaller, the discone also shows a small  $\Omega_A$  for large  $f$ , behaving like a directional antenna.

This observation is confirmed by the variation of the directivity, defined as

$$D(f) = \frac{4\pi}{\Omega_A(f)}\quad (8)$$

For the discone, the directivity starts with 3 dBi at  $f_l$  and increases with frequency to 23 dBi at the upper end of the UWB spectrum, as shown in Fig. 6b. From this result, it is clear that the discone does not behave as a constant-gain antenna over the UWB frequency range. Indeed, the discone is even more directive than the Vivaldi in the mid-band region. The increased directivity of the discone in the upper band has the positive consequence of extending the link as long as the transmitting and receiving antennas are oriented along the main beam. However, this variation in directivity can also have a significant impact on the transmitted power. The system designer must ascertain that the transmitted signal power at any frequency and angle does not exceed the EIRP regulatory limits as a result of variable directivity.



**Fig. 6** Variation of beam solid angle and directivity of UWB antennas with frequency  
a Beam solid angle  
b Directivity

The above results establish that omni-directional UWB antennas do not exhibit constant gain over the UWB band.

## 6 Waveform distortion

The effect of antennas on UWB system performance can be quantified by defining a suitable figure of merit for the quality of the communications link. We define angular bandwidth,  $B_n(\theta, \varphi)$ , as the  $n$  dB bandwidth at angular coordinates  $(\theta, \varphi)$ , where  $n$  is a suitable threshold commonly taken as 3 or 10 compared to the peak of the radiation pattern. This is the effective bandwidth perceived by a terminal in the direction specified by  $(\theta, \varphi)$ , and is a direct measure of the antenna angular-spectral dispersion.

Figure 7 shows the elevation plane angular bandwidth  $B_n(\theta, \varphi)|_{\varphi=\text{constant}}$  for the discone and Vivaldi, with the full system bandwidth  $B_{\text{max}} = 7.5$  GHz also marked for reference. Most noticeably, there is only a very small window of  $\theta$  to approach the full  $B_{10}(\theta, \varphi)$ , close to  $\theta = 50^\circ$ . This angle is significantly displaced from the equatorial plane,  $\theta = 90^\circ$ , usually deemed ideal for such omni-directional antennas, at which the half-power bandwidth  $B_{10}(\theta, \varphi)$  is less than 2 GHz. The Vivaldi antenna retains a third of its maximum  $B_{10}(\theta, \varphi)$  at all values of  $\theta$ , which amounts to partial spectral leakage in undesired directions.

Figure 8 illustrates the measured angular transfer functions of the discone antenna, given by

$$|H(\theta, \varphi, f)| = \sqrt{P_n(\theta, \varphi, f)}\quad (9)$$

at  $\theta = \{0^\circ, 30^\circ, 60^\circ, 90^\circ\}$ . The least attenuation and relative uniformity in the transfer function is observed at  $\theta = 60^\circ$ , which agrees with the conclusions drawn from Fig. 7, and therefore the least spectral distortion will be caused to the signal radiated at that angle.

The edge reflections in a finite antenna cause radiation of multiple transients whose separation varies with the look angle [38]. This can be overcome with the use of tapered resistive [39] or capacitive [40] loading. Edge reflection analysis, however, is not included in this treatment.

The response of the antenna to a signal,  $s(t)$ , is a filtering operation given by

$$R(\theta, \varphi, f) = S(f)H(\theta, \varphi, f)\quad (10)$$

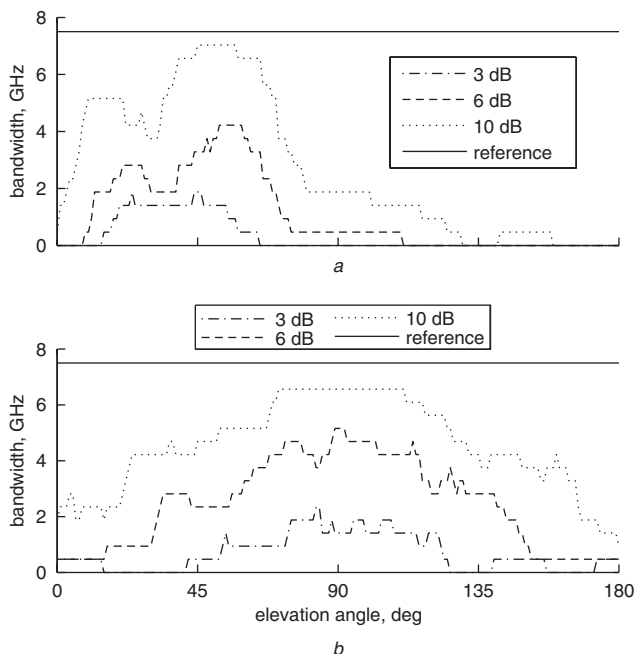


**Fig. 7** Effective angular bandwidth of discone and Vivaldi antennas in the elevation plane

The reference line indicates the full 7.5 GHz bandwidth of a UWB signal occupying the FCC UWB band, and  $\theta$  is defined as in the spherical coordinate system

*a* Discone  
*b* Vivaldi

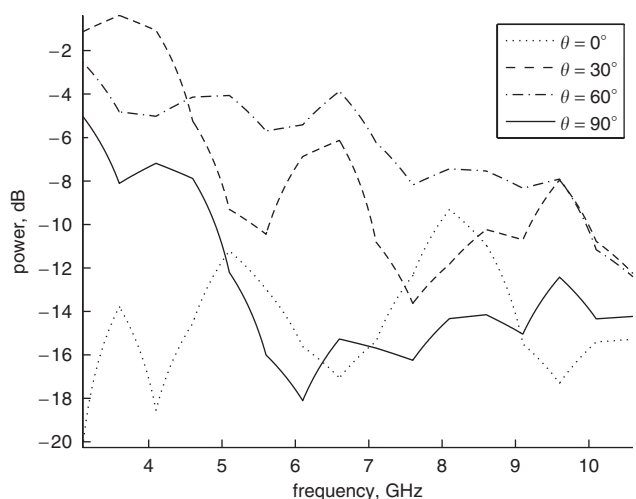


**Fig. 8** Frequency transfer function of the discone antenna at various angles of elevation, with  $\theta$  defined as in the spherical coordinate system

where  $S(f)$  is the Fourier transform of  $s(t)$  and  $R(f)$  is the spectrum of the distorted signal. The effect of antenna dispersion on a UWB signal is illustrated with the help of a Gaussian monopulse [41] commonly used in impulse radio systems [2]. The monopulse, also known as a Gaussian doublet, is the first derivative of a Gaussian pulse with a single time-domain zero-crossing and the functional form

$$s(t) = S_0 \frac{t}{\tau} e^{-\frac{t^2}{2\tau^2}} \quad (11)$$

where  $\tau$  signifies the time decay constant and  $S_0$  the amplitude. The output waveform is given by

$$r(\theta, \varphi, t) = \int_{-\infty}^{\infty} s(t - \xi) h(\theta, \varphi, \xi) d\xi, \quad (12)$$

where  $h(\theta, \varphi, t)$  represents the directional impulse response of the antenna, related to the antenna transfer function in (9) through the Fourier transform, and  $\xi$  is the integration variable.

Figure 9a shows the original monocycle  $s(t)$  with its 3 dB bandwidth satisfying the FCC UWB spectral masks, while Fig. 9b through d show the distorted waveforms  $r(\theta, \varphi, t)$ . It is seen that a discone antenna alters the pulse shape depending on the elevation angle, and the waveform at  $\theta=60^\circ$  has greater similarity to the transmitted (or template) waveform than those at  $30^\circ$  and  $90^\circ$ , owing to a flatter antenna response and wider effective bandwidth at  $60^\circ$  as discussed earlier.

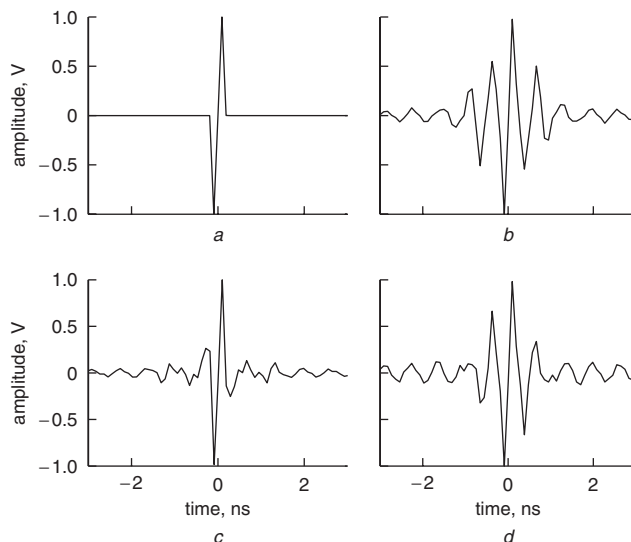


**Fig. 9** Waveform distortion by a discone antenna at various elevations

The amplitude is peak-normalised, and  $\theta$  is defined as in the spherical coordinate system

*a* Original waveform  
*b*  $\theta = 30^\circ$   
*c*  $\theta = 60^\circ$   
*d*  $\theta = 90^\circ$

The angular-spectral effects of other UWB antennas are expected to result in signal dispersion in a fashion similar to that analysed above. Also, other UWB waveforms would experience antenna distortion, and both full-band and multi-band systems would be affected. This includes the orthogonal frequency division multiplexing (OFDM) [42] or direct-sequence [43] modulated signals used in multi-carrier UWB implementations [44]. In a communications link, the signal radiated by a UWB transmitter is filtered by the antenna based on its direction-of-departure. Multipath components of this antenna-filtered signal, after transmission, may undergo a combination of various propagation mechanisms, altering its frequency content [45]. In the indoor propagation channel, a large number of multipaths reach the receiver [4, 34] with a wide range of directions-of-arrival (DOAs) [24], causing the pulse shape of each multipath arrival to be individually altered depending on its DOA [46, 47], and consequently presenting a highly distorted composite signal to the subsequent receiver components. Antenna distortion can thus degrade the signal-to-noise ratio (SNR) at the receiver considerably. In UWB signals that already operate at low SNR, this can drastically increase the outage probability and symbol error rate, reduce the capacity, and limit the coverage range.

## 7 Conclusion

It has been shown that the angular radiation properties of UWB antennas vary substantially over the frequency band. For the vertically polarised, omni-directional disccone antenna, the low frequency components of a UWB signal are radiated almost isotropically, midband frequencies are radiated in a well-defined boresight pattern in the elevation plane, while high frequencies experience beam splitting and slanting. With the directional Vivaldi antenna, there is strong low- and medium-frequency leakage off the boresight while the high frequency components achieve the desired directivity. As a reciprocal phenomenon, the frequency content of the signal radiated by these UWB antennas is a function of the look angle. This can result in unpredictable system performance in a typical short-range wireless network, in which the location of the mobile terminals is generally unknown and varying. This characterisation provides evidence for the existence of angular-spectral signal dispersion resulting from antennas, and it is established that the antenna characteristics vary jointly with frequency and direction. The boresight beamwidth of the disccone antenna falls exponentially with frequency, the beam solid angle decreases from 3.3 sr to 0.1 sr across the FCC UWB band, and its directivity increases from 3 dBi to 23 dBi. A comparison of the variation of the disccone and Vivaldi beam solid angle and directivity proves that an omni-directional antenna does not provide constant gain across the band. The effective angular bandwidth of the antennas is found to be sensitive to direction. The 10 dB bandwidth of vertically polarised disccone antennas is less than 2 GHz in the horizontal plane, severely affecting the operation of a full-band UWB system. Pulse shape distortion with look-angle is also observed as a consequence of bandwidth variation owing to antenna dispersion. These results establish the variability of antenna radiation properties over the UWB frequency range and underline the significance of this effect in system design and modelling.

## 8 Acknowledgments

This work was supported by the Engineering and Physical Sciences Research Council, UK, under grant GR/T21769/01. The authors are grateful to Dr. Ben Allen and Dr. Dominic O'Brien for their valuable comments and suggestions.

## 9 References

- 1 Win, M.Z., and Scholtz, R.A.: 'Characterization of ultra-wideband wireless indoor channels: a communication-theoretic view', *IEEE J. Sel. Areas Commun.*, 2002, **20**, (9), pp. 1613–1627
- 2 Win, M.Z., and Scholtz, R.A.: 'Impulse radio: how it works', *IEEE Commun. Lett.*, 1998, **2**, (2), pp. 36–38
- 3 'Revision of Part 15 of the Commission's rules regarding ultra-wideband transmission systems: First report and order', Federal Communications Commission, Washington, DC, USA FCC 02–48, 14 Feb. 2002
- 4 Hashemi, H.: 'The indoor radio propagation channel', *Proc. IEEE*, 1993, **81**
- 5 Malik, W.Q., Edwards, D.J., and Stevens, C.J.: 'Optimal system design considerations for the ultra-wideband multipath channel'. Proc. IEEE Veh. Technol. Conf., Dallas, TX, USA, Sep. 2005
- 6 Schelkunoff, S.A.: 'Electromagnetic waves' (Van Nostrand, Boston, USA, 1943)
- 7 Farr, E.G.: 'Optimization of the feed impedance of impulse radiating antennas, part II: TEM horns and lens IRAs', *Sensor and Simulation Note 384*, 1995, as listed at no. 55 on <http://www.farr-research.com/biblio.html>
- 8 Johnk, R.T., and Ondrejka, A.R.: 'Time-domain calibrations of d-dot sensors'. NIST Technical Note (NISTTN 1392), Feb. 1998
- 9 Gibson, P.J.: 'The Vivaldi aerial'. Proc. Eur. Microwave Conf., Brighton, UK, Sep. 1979
- 10 Andrews, J.R.: 'UWB signal sources, antennas & propagation'. Application Note AN-14a, Aug. 2003
- 11 Powell, J.: 'Antenna design for ultra wideband radio'. Masters thesis, Massachusetts Institute of Technology, 2004
- 12 Kraus, J.D.: 'Antennas' (McGraw-Hill, New York, USA, 1988, 2nd edn.)
- 13 Harmuth, H.F., and Shao, D.-R.: 'Antennas for non-sinusoidal waves - 1: Radiators', *IEEE Trans. Electromagn. Compat.*, 1983, **EMC-25**
- 14 Schantz, H.G.: 'Dispersion and UWB antennas'. Proc. IEEE Int. Workshop Ultra Wideband Sys. joint with Conf. Ultra Wideband Sys. Tech., Kyoto, Japan, May 2004
- 15 Sorgel, W., and Wiesbeck, W.: 'Influence of the antennas on the ultra-wideband transmissions', *EURASIP J. Appl. Signal Process.*, 2005, **2005**, pp. 296–305
- 16 Sorgel, W., Waldschmidt, C., and Wiesbeck, W.: 'Antenna characterization for ultra wideband communications'. Proc. Int. Workshop Ultra-Wideband Sys., Oulu, Finland, June 2003
- 17 Friis, H.T.: 'A note on a simple transmission formula', *Proc. IRE Waves Electrons*, 1946, **34**, pp. 254–256
- 18 Schantz, H.G.: 'Introduction to ultra-wideband antennas'. Proc. IEEE Ultra-Wideband Sys. Tech., Reston, VA, USA, Nov. 2003
- 19 Malik, W.Q., Edwards, D.J., and Stevens, C.J.: 'The impact of physical layer frontend characteristics on ultra-wideband radio'. Proc. Int. Conf. Telecom., Cape Town, South Africa, May 2005
- 20 Harmuth, H.F.: 'Antennas and waveguides for nonsinusoidal waves' (Academic, New York, 1984)
- 21 Kunisch, J., and Pamp, J.: 'Considerations regarding the correlation between UWB antenna transmit and receive responses'. Proc. URSI Int. Symp. Electromagn. Theory, Pisa, Italy, May 2004
- 22 Hussain, M.G.M.: 'Antenna patterns of nonsinusoidal waves with the time variation of a Gaussian pulse - Part 1', *IEEE Trans. Electromagn. Compat.*, 1988, **30**, (4), pp. 504–512
- 23 Malik, W.Q., Stevens, C.J., and Edwards, D.J.: 'Synthetic aperture analysis of multipath propagation in the ultra-wideband communications channel'. Proc. IEEE Workshop Sig. Proc. Adv. Wireless Commun., New York, USA, June 2005
- 24 Spencer, Q.H., Jeffs, B.D., Jensen, M.A., and Swindlehurst, A.L.: 'Modeling the statistical time and angle of arrival characteristics of an indoor multipath channel', *IEEE J. Sel. Areas Commun.*, 2000, **18**, (3), pp. 347–360
- 25 Chong, C.-C., Tan, C.-M., Laurenson, D.I., McLaughlin, S., Beach, M.A., and Nix, A.R.: 'A new statistical wideband spatio-temporal channel model for 5 GHz band WLAN systems', *IEEE J. Sel. Areas Commun.*, 2003, **21**, (2), pp. 139–150
- 26 King, R.W.P.: 'Theory of linear antennas' (Harvard Press, Cambridge, MA, USA, 1956)
- 27 Sandler, S.S., and King, R.W.P.: 'Compact conical antennas for wide-band coverage', *IEEE Trans. Antennas Propag.*, 1994, **42**, (3), pp. 436–439
- 28 Langley, J.D.S., Hall, P.S., and Newham, P.: 'Novel ultrawide-bandwidth Vivaldi antenna with low crosspolarisation', *Electron. Lett.*, 1993, **29**, (23), pp. 2004–2005
- 29 Fourikis, N., Lioutas, N., and Shuley, N.V.: 'Parametric study of the co- and cross-polarisation characteristics of tapered planar and antipodal slotline antennas', *IEE Proc., Microw. Antennas Propag.*, 1993, **140**, (1), pp. 17–22
- 30 Langley, J.D.S., Hall, P.S., and Newham, P.: 'Balanced antipodal Vivaldi antenna for wide bandwidth phased arrays', *IEE Proc., Microw. Antennas Propag.*, 1996, **143**, (2), pp. 97–102
- 31 Guillanton, E., Dauvignac, J.Y., Pichot, C., and Cashman, J.: 'A new design tapered slot antenna for ultra-wideband applications', *Microw. Opt. Tech. Lett.*, 1998, **19**, (4), pp. 286–289
- 32 Allen, B.: 'Antenna and propagation design challenges for ultra wideband wireless systems'. Proc. Loughborough Ant. Propag. Conf., Loughborough, UK, Apr. 2005
- 33 Liu, G., and Grimes, C.A.: 'Spherical-coordinate FDTD analysis of conical antennas mounted above finite ground planes', *Microw. Opt. Tech. Lett.*, 1999, **23**
- 34 Ghassemzadeh, S.S., Jana, R., Rice, C.W., Turin, W., and Tarokh, V.: 'Measurement and modeling of an ultra-wide bandwidth indoor channel', *IEEE Trans. Commun.*, 2004, **52**, (10), pp. 1786–1796
- 35 Sulonen, K., Suvikunnas, P., Vuokko, L., Kivinen, J., and Vainikainen, P.: 'Comparison of MIMO antenna configurations in picocell and microcell environments', *IEEE J. Sel. Areas Commun.*, 2003, **21**, (5), pp. 703–712
- 36 Balanis, C.A.: 'Antenna theory: analysis and design' (John Wiley & Sons, New York, USA, 1997)
- 37 Adachi, S., Kouyoumjian, R.G., and Sickle, R.G.V.: 'The finite conical antenna', *IRE Trans. Antennas Propag.*, 1959, **7**, (5), pp. 406–411
- 38 Maloney, J.G., Smith, G.S., and Scott, R.: 'Accurate computation of the radiation from simple antennas using the finite-difference time-domain method', *IEEE Trans. Antennas Propag.*, 1990, **38**, (7), pp. 1059–1068
- 39 Wu, T.T., and King, R.W.P.: 'The cylindrical antenna with nonreflecting resistive loading', *IEEE Trans. Antennas Propag.*, 1965, **AP-13**, (3), pp. 369–373
- 40 Rao, B.L.J., Ferris, J.E., and Zimmerman, W.E.: 'Broadband characteristics of cylindrical antennas with exponentially tapered capacitive loading', *IEEE Trans. Antennas Propag.*, 1969, **AP-17**, (2), pp. 145–151

- 41 Conroy, J.T., LoCicero, J.L., and Ucci, D.R.: 'Communication techniques using monopulse waveforms'. Proc. IEEE Conf. Mil. Comm., Atlantic City, NJ, USA, Oct. 1999, Vol. 2
- 42 Batra, A., *et al.*: 'Multiband OFDM physical layer proposal for IEEE 802.15 Task Group 3a', IEEE P802.15-03/268r0-TG3a, July 2003
- 43 Runkle, P., McCorkle, J., Miller, T., and Welborn, M.: 'DS-CDMA: the modulation technology of choice for UWB communications'. Proc. IEEE Ultra-Wideband Sys. Tech., Reston, VA, USA, Nov. 2003
- 44 Aiello, G.R., and Rogerson, G.D.: 'Ultra-wideband wireless systems', *IEEE Microw. Mag.*, 2003, 4, (2), pp. 36-47
- 45 Molisch, A.F.: 'Ultrawideband propagation channels - theory, measurement, and modeling', *IEEE Trans. Veh. Technol.*, 2005, 54, (5), pp. 1528-1545
- 46 Cramer, R.J.-M., Scholtz, R.A., and Win, M.Z.: 'Evaluation of an ultra-wide-band propagation channel', *IEEE Trans. Antennas Propag.*, 2002, 50, (5), pp. 561-570
- 47 Wilson, R.D., and Scholtz, R.A.: 'Template estimation in ultra-wideband radio'. Proc. Asilomar Conf. Signals Systems Computers, Pacific Grove, CA, USA, Nov. 2003